

Additive manufacturing of multi-material soft robot for on-demand drug delivery applications

Erina Baynojr Joyee, Yayue Pan*

Department of Mechanical and Industrial Engineering, University of Illinois at Chicago, Chicago, IL, USA



ARTICLE INFO

Keywords:

Multi-material 3D printing
Particle-polymer composite
Soft robotics
Soft manipulation
Stereolithography

ABSTRACT

Soft robotics has tremendous potential for various in-vivo bio applications. However, developing untethered soft robots is quite challenging in terms of designing robust actuation systems, efficient fabrication processes and integrating multiple functionalities. This study proposes an untethered fully 3D printed soft robot, capable of multi-modal locomotion. This soft robot has a multi-material and compliant body structure made with magnetic particle-polymer composites which can be 3D printed directly from a digital computer model. The material composition is digitally programmed for untethered magnetic actuation and the robot contains two functional parts, anterior and posterior legs, with embedded magnetic materials. The robot has 3 degrees of freedom and it is capable of bi-directional bending in xy plane and z direction. In this study, the soft robot prototypes are printed with a novel magnetic field assisted projection stereolithography (M-PSL) technique. The magnetic torque on the robot body during turning locomotion is also measured experimentally and compared with theoretical prediction. Additionally, to demonstrate the multi-functionality of the robot, a magnetically controlled drug carrier reservoir is integrated into the anterior leg of the robot. The robot can store liquid drug inside this reservoir and release the drug once it reaches the target. A dummy drug delivery application is also demonstrated inside a human stomach model and a lung model.

1. Introduction

Soft robotics is a sub-field of robotics that deals with robots made with soft and compliant materials. These robots are often inspired from biological structures to achieve desired flexibility and adaptability to dynamic environments. Such adaptive characteristics and multi-modality in soft robots can facilitate various in-vivo bio applications, such as bio sensing, minimally invasive surgery, drug delivery, enhanced bio imaging etc.

In recent years, researchers have developed different soft robots with various locomotion control systems and sensing capabilities [1,2]. These robots usually achieve the dexterity and deformability of their soft body by incorporating active sensing or implementing morphological computation. Different actuation systems integrated into soft robots in literature include pneumatic [3–7], shape memory alloy (SMA) based [8–12], hydraulic [13–15], motor-tendons [16], thermal-electroactive polymers, and magnetic actuators [17]. Hydraulic and pneumatic actuators have been widely used since they can provide powerful actuation in the soft materials [3–6,11]. However, they generally require complex fluid or air supply mechanisms including compressors or pressure regulating components. These components often limit

untethered applications and make the fabrication assembly process of the soft robot much more complicated. Another type of commonly used actuators for soft robots is SMA based actuators, which have been broadly used for developing several bio-inspired soft robots [8–11,17]. For example, Trimmer et.al [10,17] employed SMAs as actuators to design caterpillar inspired soft robots, capable of mimicking crawling and inching motions with steering abilities. However, the fabrication procedure for these soft robots was time consuming due to the manual assembly of different three dimensional (3D) printed parts. Such inefficient fabrication process also limited the achievable resolution, geometry, and overall size of the robot body. Moreover, the SMA coils require cooling down time which limits the maximum actuation frequency of the robot as well. This in turn significantly affects the overall motion and steering time of the robot. Furthermore, with the integration of a stiffness changing unit in the robot, structures actuated by hydraulic, pneumatic, SMA based or, motor-tendon based actuators become complicated and trouble prone with complex direction control. Because of external power sources and additional wires for actuation, these robots also have limited regions of applicability, especially in the sophisticated environments.

As an alternative, magnetic actuation is an untethered external field

* Corresponding author.

E-mail address: yayuepan@uic.edu (Y. Pan).

<https://doi.org/10.1016/j.jmapro.2020.03.059>

Received 23 September 2019; Received in revised form 22 January 2020; Accepted 29 March 2020

Available online 16 June 2020

1526-6125/ © 2020 The Society of Manufacturing Engineers. Published by Elsevier Ltd. All rights reserved.

based actuation technique, which can circumvent several issues associated with conventional actuation systems [18,19]. Lee et al. observed that in a standard magnetic environment, a soft robot can even operate in different mediums such as vacuum, air, and liquids [19]. However, although untethered small scale robots can easily access confined locations, they usually have limited functionalities and are incapable of navigating obstacles or adapt to changes in surface texture and materials of the surrounding environment. It is also very difficult to add multiple functionalities without complicating the geometry and fabrication process [20–26]. Hu et al. [27], for example, developed an untethered magnetically actuated soft bodied robot capable of multi-modal locomotion in congested spaces such as landing, walking, rolling, jumping and crawling. However, to incorporate different functionalities like load carrying or controlled drug delivery functions in such types of robots is extremely difficult.

One of the most potential bio applications using small scale soft robots is controlled drug delivery; yet, such applications are still very limited due to the above mentioned challenges. For example, Pirmoradi et al. [28] employed a microelectromechanical systems (MEMS) device that can be magnetically controlled for on demand targeted drug delivery in body tissues. However, the device does not have movability and it must be implanted in a specific area in the body for drug release, which makes the process invasive. Small scale untethered soft robot with drug carrying and releasing capability with an efficient actuation system would be a very attractive alternative in such applications. A multi-material soft robot with a multi-modal design can potentially achieve such multi-functionality.

Multi-material 3D printing techniques, in recent years, have provided practical solutions to address different challenges related to simple and precise fabrication [3]. With this manufacturing technique, soft actuators having a complex geometry can be printed directly with a simple fabrication process. Studies conducted by Yap et al. and Bartlett et al. [29,30] revealed the potential of 3D printed soft actuators for use in robotic applications, compared to other fabrication methods like casting and molding. Layer based multi-material 3D printing has several significant advantages as it allows pre-programmed depositions of various materials in specific locations of each layer [31]. Such pre-programmed material intelligence facilitates tremendous design flexibility to multi-functional structures and devices. Furthermore, multi-material fabrication allows control of different segments of the robot body to handle complicated tasks and integrate multiple functionalities into the robot.

Our previous study presented a magnetically actuated, monolithic and untethered soft robot, which was fabricated by multi-material additive manufacturing process with smart particle-polymer composites and locally controlled material compositions. In this previous work, our additive manufacturing technique enabled the actuation intelligence to be programmed into the robot's material design, allowing the robot to be printed directly from the digital model in one piece, without any manual assembly [32]. The printed robot had two-way linear actuation capability and employed a bio-mimetic anchor push-anchor pull locomotion strategy.

Based on this previous work, this study proposes a soft robot with a new grooved body design, with improvements in multi-modal locomotion capability (three degrees of freedom (DOF)) and functionality for performing varied tasks in dynamic environments. This multi-material, monolithic and multi-functional soft robot is fabricated with elastic polymer and magnetic nano-particles (NPs) and it demonstrates superior bi-directional locomotion capability. The locally programmed distribution of the magnetic NPs in polymer attributes to the robot's magnetic actuation intelligence that allows multiple locomotion modes including linear crawling and turning locomotion. The compliant body structure is capable of bi-directional bending in xy plane and z axis, allowing the robot to maneuver in enclosed spaces with three degrees of freedom (DOF). Along with that, the deformation profile of the robot is now more comparable to the real inchworm, showing a higher crawling

speed and increased tilt angles. These design improvements enable the robot to maneuver in complicated environments like the human stomach rugae (or gastric folds). Additionally, for showcasing the multi-modal functionality of the soft robot, a controlled dummy drug delivery application is demonstrated in this study. A drug reservoir is incorporated into the robot design for carrying and releasing drugs at targeted locations. The robot's locomotion performance, obstacle crossing capability, load carrying capacity and drug delivery capability were modeled in simulations and validated by experiments in this study.

The rest of this article is organized as follows: Section 2 describes the multi-functional soft robot design; Section 3 describes the multi-material additive manufacturing process for fabricating the soft robot; Section 4 describes the linear and turning locomotion principles; Section 5 describes different experimental results with discussion of the overall performance of the soft robot; and finally Section 6 summarizes this article and the major findings.

2. Design of multi-material soft robot for multi-modal locomotion and drug delivery application

2.1. Digital design optimization

By observing the movements of an inchworm, the robot body was divided into two parts. One is the flexible middle portion of the body and the other is the functional part which can be controlled by external magnetic fields. Based on this design strategy, four designs were created. Design 1 (M1) is a robot with uniform smooth body structure from the anterior to the posterior leg (Fig. 1a); design 2 (M2) has a body structure with two distinguished functional legs at the two ends of the robot body (Fig. 1b); design 3 (M3) has a robot body with transverse grooves at the lower surface (Fig. 1c); and design 4 (M4) has a robot body with transverse grooves on both the lower and side surfaces (Fig. 1d). The transverse grooves on the lower surface support the robot body as the secondary legs. The total length of the robot models in all designs is 40 mm. This length was chosen based on the natural observation of inchworm length and the modeled deformation to length ratio.

To achieve the highest bending angle and hence the largest locomotion capability, the four robot models were compared through an FEA study in COMSOL Multiphysics. As the color maps shown in Fig. 1, the design M4 has the highest deformation under the same amount of load in the z axis. To gain the tuning locomotion capability, the middle section of the robot was divided into segments. An FEA study was also performed in COMSOL to validate the design M4 and its effectiveness of turning locomotion under an external magnetic stimuli. The AC/DC module was used as a continuum model by following the method developed in our previous study [32].

3D air medium was set as the environment during the FEA analysis with 293.15 K temperature and with the environmental pressure set at 1 atm. The CAD design was directly imported in COMSOL by using the live link. The density and Young's modulus of the polymer were known from its material specification, which were 1.1 g/cm³ and 12 MPa, respectively. The elastic modulus and Poisson ratio (0.35 for polymer and 0.29 for composite) were set manually for polymer material and also for the particle-polymer composite. For design 4 (M4), the groove design on the side surface was tested by applying different amount of force in COMSOL simulation. Optimized depth and gap among grooves were found as 0.8 mm for the maximum bending deformation in xy plane. Simulation results are shown in Fig. 1g. In the optimized design, the robot body was divided into 9 segments on the sidewall of the body, the width of each segment was 0.8 mm with a 0.8 mm gap between them. This grooved design along with the supporting legs enabled multiple modes of locomotion including linear locomotion, crawling and rotational or tuning locomotion on the xy plane with a bending deformation in the z axis. The final optimized design for the robot is illustrated in

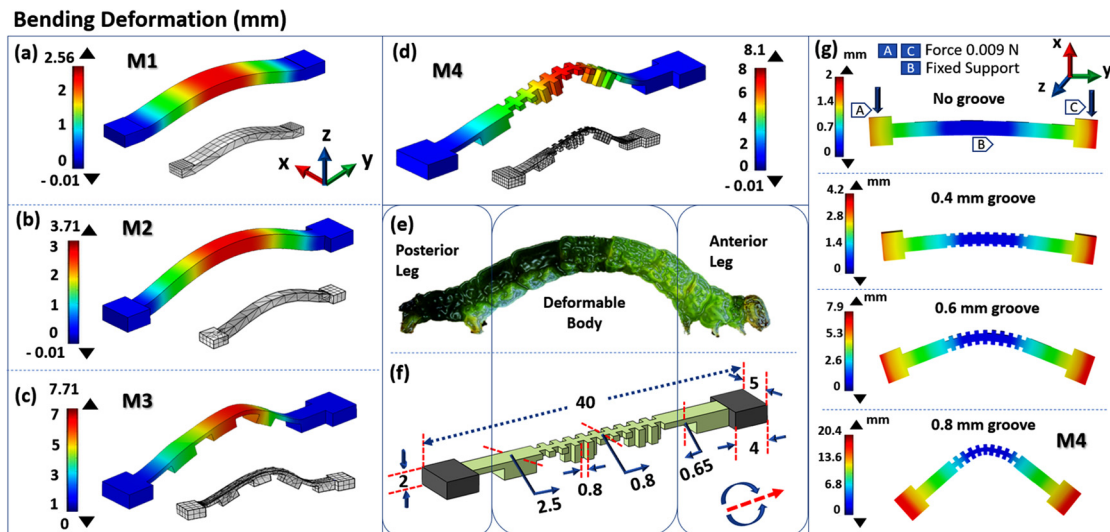


Fig. 1. Design of the particle-polymer composite soft robot. (a) Design 1 (M1): uniform smooth body structure from anterior leg to posterior leg; (b) Design 2 (M2): two distinguished functional rectangular leg at the two ends of the robot body; (c) Design 3 (M3): robot body with transverse grooves at the lower surface of the body; (d) Design 4 (M4): robot body with transverse grooves both at lower and side surfaces; (e) A real-life inchworm; (f) CAD model of the soft robot. All the dimensions are given in unit: mm. Different colors represent different material compositions in the schematic, gray: magnetic particle-polymer composite, green: flexible polymer; (g) Simulation results of the maximum deformation with different groove size on the side wall of the robot body (For interpretation of the references to colour in this figure legend, the reader is referred to the web version of this article).

Fig. 1f with all body dimensions in millimeters.

2.2. Digital design of a drug reservoir integrated in the robot body

To achieve localized and controlled drug delivery in a sophisticated environment (such as inside the human body), this study attempted to integrate a drug reservoir into the anterior leg of the robot, as illustrated in Fig. 2. The reservoir is a 3 mm (width) \times 2 mm (length) \times 1.55 mm (height) rectangular groove, positioned in the anterior leg of the robot (Fig. 2a inset). A 0.2 mm thick film is designed to cover the reservoir with a small aperture of 0.2 mm diameter on the top, from which the drug will be released on demand. The film is made of particle-polymer composites which can be triggered by an external magnetic field (\vec{H}). A TopPette Pipette with a 0.2 mm diameter micro-needle was used to fill the reservoir with drug before the drug delivery job.

To have the appropriate mechanical and magnetic properties for achieving such an on-demand drug release mechanism, the material composition needs to be locally programmed. The composite material

makes the side wall and the film of the reservoir and its aperture hydrophobic. It also increases the surface tension, which in turn generates a restrictive capillary force. Without an external force, this restrictive force prevents the drug flow from the reservoir to the outer surface. When the robot is in motion, the anterior leg is always under the influence of the external magnetic field. The skin at the lower portion of the anterior leg is deflected and a tension force towards the magnet is created, as shown in Fig. 2b. Once the robot reaches the target, the magnetic field is switched off. As a result, the deformed bottom of the reservoir goes back to its normal position and creates an up-thrust pressure to the liquid drug. This pressure overcomes the restrictive capillary force and as a result, releasing the drug from the aperture, as illustrated in Fig. 2c. The releasing time and speed can be manipulated by controlling the strength and the on-off duration of the external magnetic field.

3. Additive manufacturing of the multi-material soft robot

A multi-material additive manufacturing process, magnetic field assisted projection stereolithography (M-PSL), was developed and used to print the designed soft robot prototypes in Figs. 1f and 2a. This multi-material AM process is capable of fabricating smart composite structures directly from a digital model in a layer by layer manner. Fig. 3a shows the user interface of the software to control the M-PSL process. The M-PSL setup is shown in Fig. 3b. A digital micro-mirror device (DMD) with 1024 \times 768 pixel resolution was used as a light source. The envelope size was set as 42.7 mm \times 32 mm in the printing system and the effective light wavelength of the imaging unit was 380–420 nm. The details of the printing procedure of the soft robot and other parameters are the same as the ones described in our previous study [32,33].

A non-aqueous photocurable resin Spot E elastic from Spot A Material, (Sonnaya Ulitka S.L., Barcelona, Spain) was used as a base polymer matrix. This resin had translucent color and a good elasticity which allowed the cured composite of this material to bend or deform very easily [34]. Dry magnetic nanoparticles (EMG 1200) with a 10 nm nominal diameter from Ferrotec (NH, USA) was used as the magnetic filler material for printing the functional parts of the robot. EMG 1200 contains 67–80 % w/w of iron oxide with 50–70 emu/g saturation

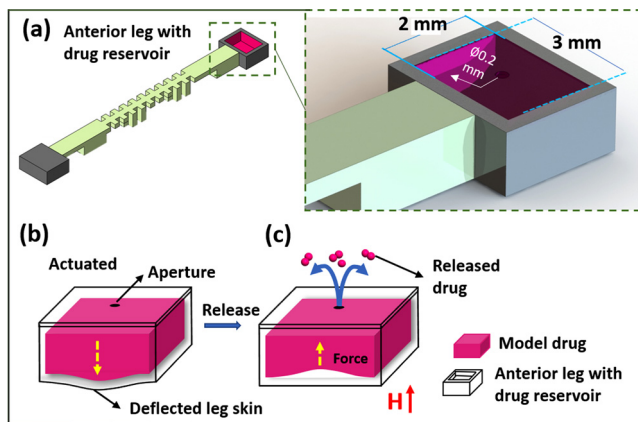


Fig. 2. (a) Design of drug reservoir in the anterior leg; (b) Magnetic field from the anterior magnet creating deflection of the leg skin towards the magnet; (c) Drug released through the small aperture after the anterior magnetic field is turned off.

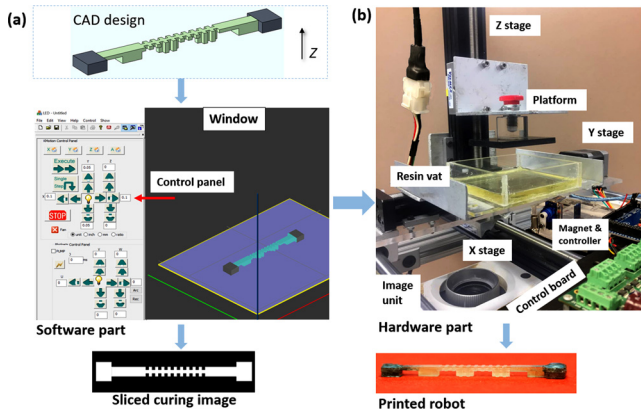


Fig. 3. (a) Software interface to control the M-PSL prototype; (b) The M-PSL hardware prototype and printed robot.

magnetization. For printing the robot layer, the fabrication process begins with depositing magnetic particles into the resin vat by using a programmed dispensing system. An external rotating magnetic field attracts the particles to the robot leg printing area. After the particles are distributed in the right regions with the appropriate concentration, a mask image of the corresponding layer is projected through the imaging unit. The appropriate curing time for each layer with different material compositions was investigated in our previous study [31,33].

After that, the curing image of the entire cross-sectional plane of that layer is illuminated. If the layer does not comprise particles, the image is projected to the liquid resin vat directly for a specific curing time after re-coating the new layer of liquid polymer resin between the previously printed part or platform (if the first layer) and the base of the resin vat. The platform separates the newly cured layer from the base of the resin vat. A new layer of liquid resin fills the gap between the bottom surface of the vat and the printed layer for the next layer fabrication. A microcontroller is used to control both the rotating magnetic field and movement of z axis. After the printing, the printed robot is rinsed with ethyl alcohol and then kept inside an ultraviolet chamber for 20 min to relieve any remaining residual stress.

4. Locomotion analysis of the multi-material soft robot

4.1. Linear locomotion

The linear locomotion principle of the soft robot is inspired by the push-pull locomotion strategy of the inchworm [10,32]. An inchworm creates an alternating low and high friction states with the underlying surfaces during locomotion with their legs and body muscles named sarcomeres. Inspired by the inchworm, the proposed soft robot also creates a low-high friction state with the surface and create a similar push-pull motion. When the robot is in the rest position (Fig. 4a), both anterior and posterior legs construct a high friction with the underlying surface. Two magnets are placed underneath the two legs of the robot shown in Fig. 4a. The crawling cycle begins with the mechanical movement of the posterior magnet (magnet 1) along y axis. The posterior leg of the robot starts moving as magnet 1 pulls it forward. At the same time, the anterior magnet (magnet 2) helps the anterior leg to anchor on the underlying surface. As shown in Fig. 4 (b, inset), the robot body thus creates a bending deformation in z axis with a tilt angle (θ), with the substrate.

When the external magnetic field is absent, because of the robot body's elasticity and gravitational potential energies, the body would return to its original rest position. When the tilt angle θ reaches the maximum position (marked as a threshold angle θ_{max}), the robot body has the minimum friction with the substrate. At θ_{max} , magnet 2 starts to move forward in y direction. While the magnet 2 moves and pulls the

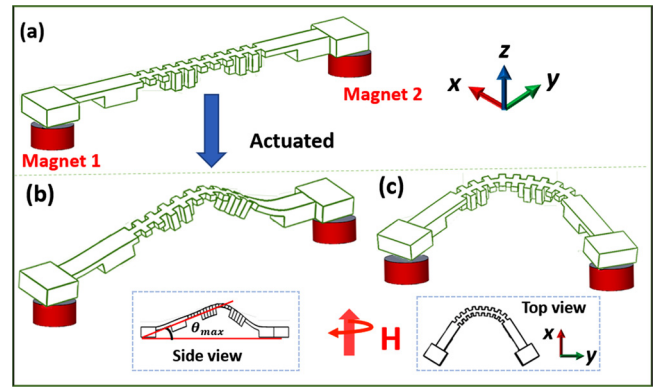


Fig. 4. Schematic showing posterior and anterior leg movement along with magnets placed beneath the two legs: (a) Resting state; (b) Linear locomotion state; (c) Turning locomotion state.

anterior leg of the robot with it, magnet 1 holds the posterior leg and acts as an anchor. The tilt angle gets smaller and when it becomes zero the anterior leg stops moving and the body returns to its original rest position. The magnet 1 then starts moving again for a new locomotion cycle.

The tilt angle was measured by analyzing the videos using MATLAB functions and ImageJ. The maximum tilt angle (θ_{max}) of the robot in z axis is measured to be 22° , improved from the 12° of the previous design [32]. It resembles the real life inchworm tilt angle 25° much more closely. Compared to the previous robot which has no groove integrated [32], the deformation of the body in z axis is also improved from 4.5 to 5.5 mm and the linear speed of the robot is increased from 1.67 mm/s to 3.1 mm/s.

4.2. Turning locomotion

As discussed in Section 2, with the new groove segment design, the robot is capable of bending and hence turning freely in xy plane.

The turning locomotion principle follows a similar strategy to the linear locomotion, by utilizing an external magnetic field to manipulate the anterior and posterior legs. To make a turn in x or y axis, the external anterior magnet is moved mechanically along the direction. Following its direction, the anterior leg also moves forward to make the turn. During this time, the posterior magnet remains in its position, acting as an anchor holding the posterior leg. The robot body is thus bent in the xy plane. At the desired bending angle, the posterior magnet is used to move the body to its normal position (0° deflection in xy plane). There is no z axis deflection of the robot body during the turning locomotion. After turning, the robot continues its linear locomotion using crawling cycles to reach the desired location.

Experiments were conducted to observe the tuning locomotion dynamics of the printed robot. As the anterior magnet moves to the target location (blue dot in Fig. 5a), the anterior leg of the robot follows the trajectory in xy plane. This movement creates a magnetic torque on the robot body which deflects the anterior leg towards the anterior magnet. The magnetic torque applied on the robot body can be theoretically calculated in terms of magnetic moment m and magnetic flux intensity B ,

$$\begin{aligned} T_m = m \times B = (m_y \cdot B_z - m_z \cdot B_y) \bar{I} + (m_z \cdot B_x - m_x \cdot B_z) \bar{J} \\ + (m_x \cdot B_y - m_y \cdot B_x) \bar{K} \end{aligned} \quad (1)$$

Eq. (1) can be simplified, as the robot body only moves in the xy plane during turning locomotion. Let the deflection angle between y axis and anterior leg is θ_i , the torque can be calculated with,

$$T_m = m \cdot B \cdot \sin \theta_i \quad (2)$$

With the residual flux density (B_r), permeability in vacuum (μ) and

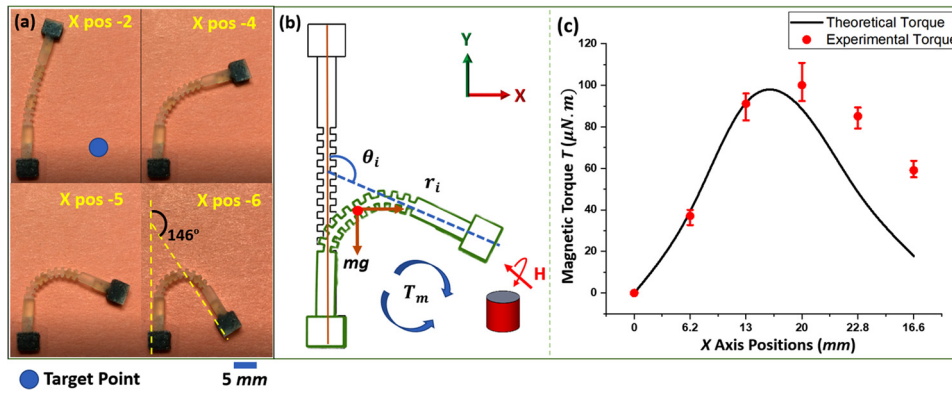


Fig. 5. A turning locomotion example. (a) Soft robot deflection in the xy plane during turning locomotion; (b) Displacement of anterior leg in x and y axis with corresponding deflection angle; (c) Comparison of theoretical and experimental torque of the soft robot.

volume of the magnetic segment (V), the magnetic moment (m) can be computed by using the following equation, $m = \frac{1}{\mu} B_r V$. So the theoretical torque is,

$$T_m = \frac{1}{\mu} B_r \cdot V \cdot B_{xy} \cdot \sin\theta_i \quad (3)$$

The magnetic field used for this experiment has a residual flux density of 1.48 T and vacuum permeability of $\mu = 4\pi \times 10^{-7} \text{H/m}$. The theoretical torque was calculated by using Eq. (3) and compared with the experimental one. The experimental torque on the robot body at different deflection angles was measured by considering the corresponding net displacement (r_i) and magnetic force (F_m). Fig. 5b shows the displacement, deflection angle (θ_i) and magnetic torque (T_m) relative to the body axis. Fig. 5c shows the comparison between theoretical and experimental torques.

From the experiments shown in Fig. 5a, it can be observed that the robot can deflect up to a maximum of 146° in xy plane. The classical Euler-Bernoulli equation was used to measure the experimental torque at different locomotion stages while turning [35]. To use the classical Euler-Bernoulli equation, the soft robot is considered as a rectangular beam with height h and width w . The torques are then calculated as a function of cross-sectional area, second moment of inertia, Young's modulus of the composite polymer and the bending angle in each x axis position.

From the comparison results between theoretical and experimental torque values shown in Fig. 5c, it can be observed that the experimental torque values follow a similar trend as the theoretical torque, but they are comparatively higher in some positions. It's because the theoretical torque model considers the ideal standard elastic property. But for the printed soft robot, the highly elastic polymer body with the segmented grooved design results in an even higher elasticity. Due to this compliant and flexible characteristic, the deflection angle is observed to be higher during the experiments, resulting in higher net displacements and experimental torque values.

5. Experimental results and discussions

To validate the robot design and its untethered actuation mechanism effectiveness for moving and working inside confined and complicated spaces, test cases were performed in human stomach and lung models. The pathway from the human throat to the stomach (esophagus) has a diameter of only 13 mm–30 mm. In contrary, the maximum width of the robot is about 5 mm and its maximum bending height is 5.5 mm in z direction.

The high deflecting and bending capability of the robot increase its potential to maneuver in enclosed and narrow spaces. To assess the performance of the soft robot, the locomotion and drug delivery capability were tested inside an anatomical human size stomach model

(Fig. 6). The robot was carrying the liquid drug in its body-integrated reservoir, as shown in Fig. 6b. The stomach model had gastric folds making its inner structure rough, uneven and unstructured. The target was a cancer tissue placed within the folds (white tissue in the Fig. 6). A moving magnetic field generated by a permanent magnet moving beneath the stomach model was used for guided actuation of the robot.

The robot began its locomotion from the esophagus and ended up at the target tissue. During the journey from the tube to the target, the whole locomotion process can be divided into four steps by several transition points: ingress; stepping down; approaching; and release. At the beginning of its journey (Fig. 6a: Step 1: Ingress; and Fig. 6b: Step 2: Stepping down), the robot crawled through the esophagus and then stepped down to the stomach base surface. The robot bent its body downwards to make turning locomotion and this motion mechanism helped the robot to avoid spilling the drug. During the journey (Fig. 6c: Step 3: Approaching), with different combination of locomotion modes, the robot was able to travel 93 mm (from the esophagus to targeted cancer cells) distance through different rough and uneven surfaces. The experiment was repeated several times and the average speed was measured to be 3.1 mm/s.

As the robot reached the target (Fig. 6d: Step 4: Release), the anterior magnet was turned off. This created an up-thrust pressure inside the reservoir, which created an upward force. This force pushed the drug and released it through the aperture. The maximum amount of liquid drug the reservoir could carry was about $\approx 6\%$ of its own volume. The robot could not only carry and deliver the liquid drug, but it was also capable of pulling a load such as a solid pill with its body. Multiple experiments were conducted with different loads and it was observed that, on a flat surface, the robot could carry a load more than 13 times of its own weight (0.23 g). Fig. 6c shows the robot carrying a medical capsule of 3 g and moving inside the stomach model.

Another potential application with the robot's drug delivery capability was demonstrated inside the lungs. The human bronchiole structures are meshed and enclosed, which makes it congested with sharp angles in the airways, making it quite challenging to maneuver the robot along this kind of narrow spaces. The bending capability in xy plane improves the overall locomotion performance of the soft robot. In congested spaces (i.e. mazes as shown in previous work [32]), without bending capability in xy plane, the robot needs a lot of space to make a turn. Compared to the robot design in our previous work which has no bending capability, this groove-based robot design gives us a maximum bending of 146° , allowing smooth movements in congested curly spaces like human esophagus. To test the proposed soft robot, an experiment was designed with a 2D map of a human lung with tree-like branch structures. With external magnetic field assisted actuation, the robot successfully maneuvered inside the lung branches by bending its body in z axis and xy plane with a combination of linear and turning locomotion (Fig. 7)

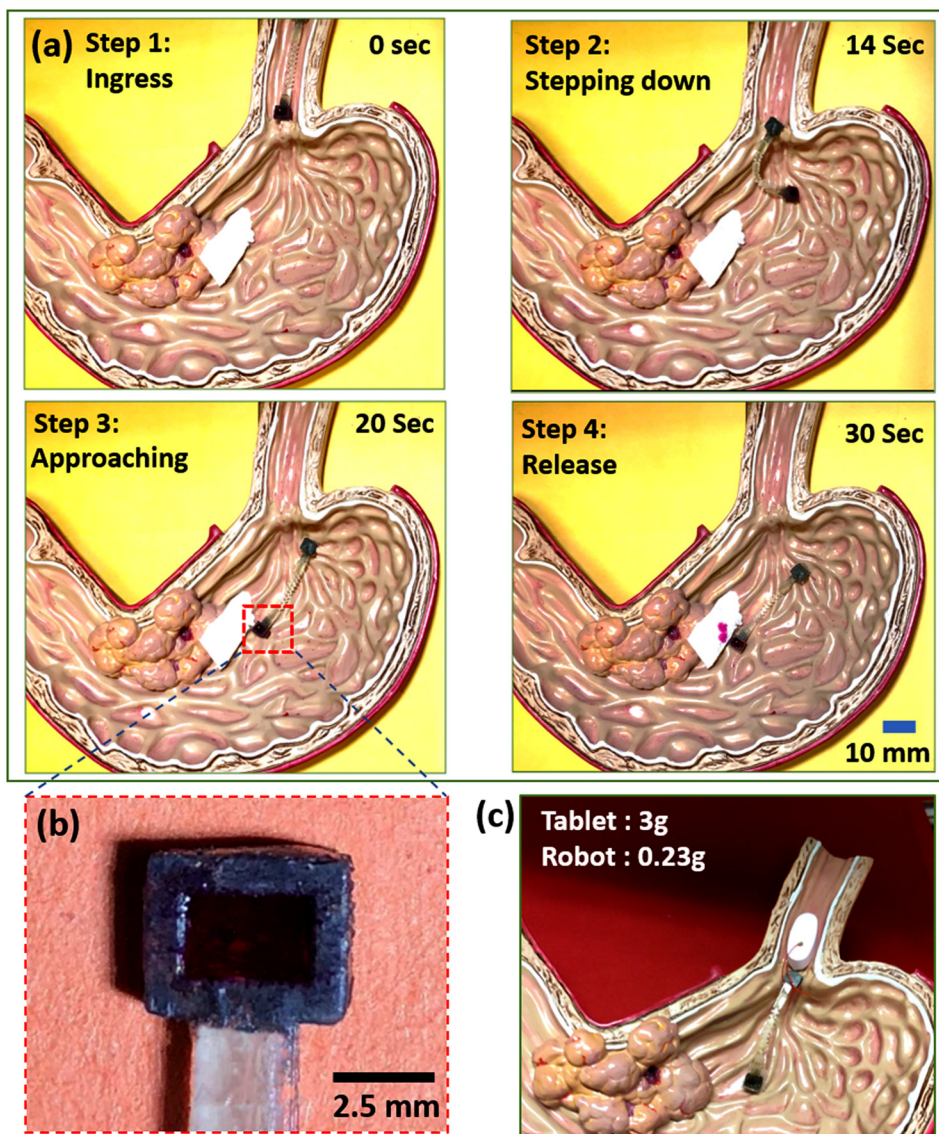


Fig. 6. (a) The multi-material soft robot crawling inside an anatomical stomach model with cancer tissue (target) and screen shots of the video that the robot entered into the stomach, moved to the targeted tumor location, and released the drug; (b) Reservoir in the anterior leg; (c) The robot can also carry a solid tablet as load.

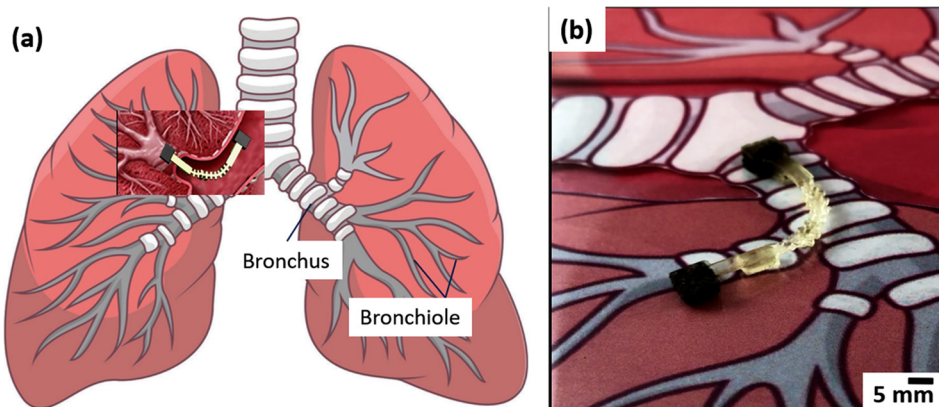


Fig. 7. (a) Schematic diagram of turning locomotion scenario in human lung; (b) The multi-material soft robot turning locomotion demonstrated on a 2D map of bronchiole network inside the human lung.

6. Conclusion

In this study, a multi-material soft robot was designed, and 3D printed, which is characterized with multi-modal locomotion capability. A multi-material M-PSL printing process was used to fabricate the robot with composition of polymer matrix and preprogrammed magnetic material distribution.

Compared to the mono-directional soft robot developed in our previous study, this study investigates a groove design for achieving bi-directional locomotion with multiple functionalities for performing tasks in harsh environments. The transverse grooves on both the lower and side surface of the robot body allows superior bi-directional locomotion capability, showing a maximum tilt angle of 22° in the z axis and 146° degrees on the xy plane. A finite element analysis model was developed in the COMSOL software and the groove design parameter settings were optimized to maximize the overall compliance of the soft robot body. The excellent compliance and the bi-directional locomotion allows the robot to crawl smoothly in congested spaces like the human esophagus or lung. An average speed of 3.1 mm/s was recorded throughout the locomotion on uneven surface. During the turning locomotion, the magnetic torque implemented on the robot body was also measured and it agreed well with theoretically calculated values. In addition to the superior multi-modal locomotion capability, the robot also has multi-functionality, as demonstrated by conducting drug delivery experiments in stomach and lungs models. For the targeted liquid drug delivery experiments, a magnetically controlled drug reservoir was integrated into the anterior leg of the robot. It has the capability of carrying the liquid drug, with a maximum volume of \approx 6% of the robot body volume. It can carry the liquid drug without spilling and deliver at the targeted place on demand. Additionally, it can also carry loads (e.g., solid drug) with its body, with a maximum weight of 13 times of its own weight.

Future work will focus on improving the adaptability of the robot. More design study will be conducted to improve the locomotion adaptability and gripping mechanism of the robot leg with the substrate. Biocompatible materials will be tested for fabricating the robot for demonstrating applications inside living organisms.

Declaration of Competing Interest

The authors declare no conflict of interest.

Appendix A. Supplementary data

Supplementary material related to this article can be found, in the online version, at doi:<https://doi.org/10.1016/j.jmapro.2020.03.059>.

References

- [1] Ghosh A, Yoon C, Ongaro F, Scheggi S, Selaru FM, Misra S, et al. Stimuli-responsive soft untethered grippers for drug delivery and robotic surgery. *Front Mech Eng* 2017;3:7.
- [2] Pfeifer R, Lungarella M, Iida F. Self-organization, embodiment, and biologically inspired robotics. *Science* 2007;318:1088–93.
- [3] Shepherd RF, Ilievski F, Choi W, Morin SA, Stokes AA, Mazzeo AD, et al. Multigait soft robot. *Proc Natl Acad Sci* 2011;108:20400–3.
- [4] Stokes AA, Shepherd RF, Morin SA, Ilievski F, Whitesides GM. A hybrid combining hard and soft robots. *Soft Robot* 2014;1:70–4.
- [5] Yang Y, Chen Y, Li Y, Chen MZ, Wei Y. Bioinspired robotic fingers based on pneumatic actuator and 3D printing of smart material. *Soft Robot* 2017;4:147–62.
- [6] Zou J, Lin Y, Ji C, Yang H. A reconfigurable omnidirectional soft robot based on caterpillar locomotion. *Soft Robot* 2018;5:164–74.
- [7] Habibi H, Land P, Ball MJ, Troncoso DA, Branson III DT. Optimal integration of pneumatic artificial muscles with vacuum-jammed surfaces to characterise a novel reconfigurable moulding system. *J Manuf Process* 2018;32:241–53.
- [8] Koh J-S, Cho K-J. Omega-shaped inchworm-inspired crawling robot with large-index-and-pitch (LIP) SMA spring actuators. *IEEE/ASME Trans Mechatronics* 2013;18:419–29.
- [9] Lee D, Kim S, Park Y-L, Wood RJ. Design of centimeter-scale inchworm robots with bidirectional claws. 2011 IEEE International Conference on Robotics and Automation (ICRA). 2011. p. 3197–204.
- [10] Umedachi T, Vikas V, Trimmer B. Softworms: the design and control of non-pneumatic, 3D-printed, deformable robots. *Bioinspir Biomim* 2016;11:025001.
- [11] Villanueva A, Smith C, Priya S. A biomimetic robotic jellyfish (Robojelly) actuated by shape memory alloy composite actuators. *Bioinspir Biomim* 2011;6:036004.
- [12] Estelle K, Blair D, Evans K, Gozen BA. Manufacturing of smart composites with hyperelastic property gradients and shape memory using fused deposition. *J Manuf Process* 2017;28:500–7.
- [13] Lin H-T, Slate DJ, Paetsch CR, Dorfmann AL, Trimmer BA. Scaling of caterpillar body properties and its biomechanical implications for the use of a hydrostatic skeleton. *J Exp Biol* 2011;214:1194–204.
- [14] Onal CD, Rus D. Autonomous undulatory serpentine locomotion utilizing body dynamics of a fluidic soft robot. *Bioinspir Biomim* 2013;8:026003.
- [15] Zatopa A, Walker S, Menguc Y. Fully Soft 3D-Printed electroactive fluidic valve for Soft hydraulic robots. *Soft Robot* 2018.
- [16] Vikas V, Cohen E, Grassi R, Sozer C, Trimmer B. Design and locomotion control of a Soft robot using friction manipulation and motor-tendon actuation. *IEEE Trans. Robotics* 2016;32:949–59.
- [17] Trimmer B. A journal of soft robotics: why now? 140 Huguenot Street, 3rd Floor New Rochelle, NY 10801 USA: Mary Ann Liebert, Inc.; 2014.
- [18] Cugat O, Delamare J, Reyne G. Magnetic micro-actuators and systems (MAGMAS). *IEEE Trans Magn* 2003;39:3607–12.
- [19] Lee H, Kim J, Kim J, Chung SE, Choi S-E, Kwon S. Programming magnetic anisotropy in polymeric microactuators. *Nat Mater* 2011;10:747.
- [20] Diller E, Sitti M. Three-dimensional programmable assembly by untethered magnetic robotic micro-grippers. *Adv Funct Mater* 2014;24:4397–404.
- [21] Diller E, Zhuang J, Zhan Lum G, Edwards MR, Sitti M. Continuously distributed magnetization profile for millimeter-scale elastomeric undulatory swimming. *Appl Phys Lett* 2014;104:174101.
- [22] Huang H-W, Sakar MS, Petruska AJ, Pané S, Nelson BJ. Soft micromachines with programmable motility and morphology. *Nat Commun* 2016;7:12263.
- [23] Koh J-S, Yang E, Jung G-P, Jung S-P, Son JH, Lee S-I, et al. Jumping on water: surface tension-dominated jumping of water striders and robotic insects. *Science* 2015;349:517–21.
- [24] Maeda S, Hara Y, Sakai T, Yoshida R, Hashimoto S. Self-walking gel. *Adv Mater* 2007;19:3480–4.
- [25] Miyashita S, Guitron S, Ludersdorfer M, Sung CR, Rus D. An untethered miniature origami robot that self-folds, walks, swims, and degrades. *Robotics and Automation (ICRA), 2015 IEEE International Conference on*. 2015. p. 1490–6.
- [26] Yuk H, Kim D, Lee H, Jo S, Shin JH. Shape memory alloy-based small crawling robots inspired by *C. Elegans*. *Bioinspir Biomim* 2011;6:046002.
- [27] Hu W, Lum GZ, Mastrangeli M, Sitti M. Small-scale soft-bodied robot with multi-modal locomotion. *Nature* 2018;554:81.
- [28] Pirmoradi FN, Jackson JK, Burt HM, Chiao M. A magnetically controlled MEMS device for drug delivery: design, fabrication, and testing. *Lab Chip* 2011;11:3072–80.
- [29] Bartlett NW, Tolley MT, Overvelde JT, Weaver JC, Mosadegh B, Bertoldi K, et al. A 3D-printed, functionally graded soft robot powered by combustion. *Science* 2015;349:161–5.
- [30] Yap HK, Ng HY, Yeow C-H. High-force soft printable pneumatics for soft robotic applications. *Soft Robot* 2016;3:144–58.
- [31] Lu L, Joyee EB, Pan Y. Correlation between microscale magnetic particle distribution and magnetic-field-Responsive performance of three-dimensional printed composites. *J Micro Nano-manuf.* 2018;6:010904.
- [32] Joyee EB, Pan Y. A fully three-dimensional printed inchworm-inspired Soft robot with magnetic actuation. *Soft Robot* 2019.
- [33] Joyee EB, Lu L, Pan Y. Analysis of mechanical behavior of 3D printed heterogeneous particle-polymer composites. *Compos Part B Eng* 2019.
- [34] Lu L, Tang X, Hu S, Pan Y. Acoustic field-assisted particle patterning for smart polymer composite fabrication in stereolithography. *3D Print Addit Manuf* 2018;5:151–9.
- [35] Lu H, Zhang M, Yang Y, Huang Q, Fukuda T, Wang Z, et al. A bioinspired multi-legged soft millirobot that functions in both dry and wet conditions. *Nat Commun* 2018;9:3944.